Advances in Civil Engineering

WILEY

RESEARCH ARTICLE OPEN ACCESS

Analysis of Underground Cavern Surrounding Rock Stability and Anchoring Effects Under High Stress Using an Optimized DDARF Method

Hai-Ping Ma[1] | Nik Norsyahariati Nik Daud[2] | Liang-Liang Yu[1]

[1]School of Civil and Architecture Engineering, Panzhihua University, Panzhihua 617000, Sichuan Province, China | [2]Department of Civil Engineering, Faculty of Engineering, Universiti Putra Malaysia, Serdang 43400, Selangor, Malaysia

Correspondence: Nik Norsyahariati Nik Daud (niknor@upm.edu.my)

Received: 11 April 2025 | **Revised:** 14 May 2026 | **Accepted:** 11 June 2026

Academic Editor: Nicola Cavalagli

Keywords: bolt | deformation | discontinuous deformation analysis for rock failure | failure process | surrounding rock stability

ABSTRACT

This study focuses on the stability of surrounding rock (SR) in underground cavities of China's western high-stress regions, using the tailwater pressure–regulating chamber of a hydropower station on the lower Jinsha River as the case. Models with and without bolts are established for excavation simulation. Based on the key assumptions of linear elastic rock blocks, fully bonded bolt–rock interface, and instantaneous excavation unloading, results show that SR failure follows a vault → walls → floor sequence consistent with excavation order. Bolts significantly enhance stability: They reduce fractured zone depth (defined as the maximum distance from excavation boundary to continuous fractured network) by 33.33% in the vault and right wall (from 6 to 4 m) and 25% in the left wall (from 8 to 6 m). For displacement (measured as absolute movement of key monitoring points relative to initial state), bolts achieve an 86.96% reduction in vault settlement (from 93.64 to 12.21 mm) and 71.38% reduction in right wall convergence (from 21.63 to 6.19 mm). However, the F1 structural plane limits bolt effectiveness on the left wall and floor, where fractured zone depth remains unchanged at 2 m. This study provides scientific support for support design in high-stress underground projects.

1 | Introduction

In recent years, China has successfully implemented numerous large-scale hydropower projects in Yunnan, Guizhou, Sichuan, and Tibet [1]. These projects have greatly promoted the rapid development of hydro-related rock mechanics and geotechnics in hydraulic engineering. In these regions, some hydropower stations feature underground caverns. However, in complex geological conditions, the surrounding rock (SR) of underground caverns is subjected to extremely high initial in situ stresses during construction and excavation. Under high-stress conditions, the stability of the SR becomes a critical issue that requires close attention [2]. The SR exhibits various forms of deformation and failure, including unloading rebound, plate spalling, and rock splitting [1]. Such damage can lead to significant financial losses and project delays. Factors like stress redistribution in the SR, the structure and size of the cavern, the excavation duration, and the strength of the cavern support can all contribute to the deformation and failure of the SR under high-stress conditions [2]. For instance, during the construction of the underground powerhouse at the Dagangshan Hydropower Station, the basalt dam top plate collapsed, with a volume of 3000 cubic meters, which adversely affected the construction schedule and safety [3, 4]. Similarly, during the excavation process at the Jinping

Hydropower Station, events such as plate separation, significant relaxation of the SR, and rock bursts occurred, all of which hindered construction progress and posed safety risks [5, 6].

As hydropower resources are extensively developed in China's western regions, there is a growing trend of undertaking underground cavern projects in mountainous and canyon areas with high geostress [7]. Consequently, deformation, failure, and instability of SR caused by high-stress conditions have become key issues in rock mechanics research and engineering practice [8]. Due to the construction of large-scale underground projects, extensive experience has been accumulated in designing SR support systems under high-stress conditions [9].

Zhang et al. [10] utilized in situ monitoring data and numerical simulations to outline the SR failure characteristics at the Guandi Hydropower Station under high-stress conditions. Xu et al. [11], Cheng et al. [12], and Ma et al. [13] integrated laboratory tests, theoretical analyses, numerical simulations, and field monitoring to investigate the SR deformation and failure properties at the Jinping Hydropower Station. They highlighted the significant impacts of weak structural planes and time-dependent deformation and advocated for dynamic support design. Feng et al. [14] employed photogrammetry and digital imaging techniques to study the spalling failure mechanisms of tunnel SR. Based on their findings, they proposed a support strategy for excavation in high-risk areas. Zheng et al. [15] compiled SR support design data from over 20 large underground caverns in China. Through statistical analysis and curve fitting, they developed an empirical formula linking geostress, cavern span, rock parameters, and SR support strength. They further proposed a support index and an evaluation method for support design rationality. Additionally, Xiao et al. [16] analyzed the failure zones of the underground powerhouse at the Lianghekou Hydropower Station using microseismic monitoring data and developed deformation alerts for SR. Li et al. [17] used three-dimensional numerical modeling of a single medium to provide a theoretical basis for cavern excavation and support. Currently, research on the deformation and failure of cavern groups under high stress mainly focuses on deformation and failure mechanisms [18–21], construction-period reinforcement measures [10, 12, 22–30], and aging deformation characteristics. However, research on deformation reduction measures remains limited. The analysis of underground cavern SR stability represents a typical nonlinear mechanical challenge, characterized by significant displacement, discontinuous changes, and inhomogeneous deformation. These factors make calculation and analysis extremely complex [31–34]. Nevertheless, continuous advancements in computer technologies have significantly propelled the development of rock mechanics research, enhancing theoretical foundations and technical methods. A variety of methods are now available for studying underground cavern SR stability, with new research techniques emerging over time [35–38]. Among these methods, numerical simulation analysis stands out as it can predict stress distribution and SR stability by simulating engineering prototypes through numerical analysis software. This method has proven invaluable in addressing geotechnical engineering challenges under complex geological conditions, primarily due to its advantages of time reduction, cost savings, and simplified operations [39]. In recent years, the rapid development of artificial intelligence/machine learning (AI/ML), digital twins (DTs), and building information modeling (BIM) technologies has provided new paradigms for stability analysis and support design optimization in underground engineering. Sharafat et al. [40] proposed a five-dimensional DT–driven stability optimization framework for large underground caverns, which enables adaptive optimization of support systems and continuous deformation monitoring by integrating real-time sensor data and virtual simulations. Tanoli et al. [41] developed a multimodel BIM framework that realizes the full-process digital transformation of large complex underground caverns from design to construction, solves the data interoperability problem in underground engineering by extending the IFC standard, and achieves a 12.4% reduction in rock bolt usage and a 9.8% reduction in shotcrete volume in the Neelum-Jhelum Hydropower Project powerhouse cavern. Muhammad Waleed et al. [42] developed a BIM-based tunnel information modeling prototype, providing a feasible solution for standardized data management in the tunnel design stage. In terms of construction decision support, Sharafat et al. [43] proposed a DT-driven blast design optimization method for underground construction, while Sharafat et al. [44] established a BIM-IFC standard data model framework for rock support in drill-and-blast tunneling projects, laying the foundation for digital management of support systems. Although these advanced methods have made significant progress in data integration, real-time monitoring, and collaborative design, most of them are based on continuum mechanic assumptions and cannot accurately simulate discontinuous fracture propagation, block movement, and the complex interaction between bolts and rock mass commonly encountered in high-stress hard rock conditions. To address this challenge, various numerical methods have been developed, including the finite element method (FEM) and finite difference method (FDM), which have been widely used in underground engineering. However, these methods still have limitations in dealing with discontinuous rock mass failure problems. Therefore, this study adopts the Optimized Discontinuous Deformation Analysis for Rock Failure (O-DDARF) method to more accurately simulate the SR failure process and bolt reinforcement effect of high-stress underground caverns.

Rock is a geological material full of discontinuities, and discontinuous deformation is a characteristic of rock deformation and failure. Discontinuous Deformation Analysis (DDA) simulates rock's discontinuous deformation [45]. Jiao et al. proposed the DDA for Rock Failure (DDARF) method within the DDA framework, which can simulate the entire jointed rock mass failure process [45, 46]. However, DDARF can only generate uniform grids, leading to excessive computational load and prolonged calculation time for large projects, restricting its applicability [47, 48]. To address this, Ma and Daud [49] improved DDARF to generate heterogeneous grids, developing the O-DDARF. This method flexibly generates grids of varying sizes, maintaining accuracy while enhancing efficiency, making it suitable for broad engineering analysis.

This study uses the O-DDARF method to analyze the bolt action on the SR under high stress. It provides scientific references for constructing underground projects like large hydropower stations and large-span traffic tunnels. The main contributions of this study are threefold.

1. It applies the O-DDARF method with heterogeneous meshing to high-stress underground cavern analysis,

demonstrating its ability to capture detailed fracture propagation with a 50% higher computational efficiency than traditional uniform-grid DDARF.

2. It quantitatively evaluates the reinforcing effect of rock bolts under the influence of a dominant structural plane (F1), revealing that bolt effectiveness varies significantly across different cavern sections due to structural plane control.
3. It provides a systematic comparison of fractured zone depth and displacement responses to bolting, clarifying their different mechanical implications for long-term stability assessment.

2 | Method

2.1 | Fundamentals of the DDA Method

DDA describes the displacement and deformation of any point in a block using a complete first-order approximate displacement polynomial [45]:

$$u = a_1 + a_2 x + a_3 y + a_4 xy$$
$$v = a_5 + a_6 x - a_2 y + a_3 xy$$

where (u, v) is the displacement of the point, and $a_1 - a_6$ are undetermined coefficients. Each block has six degrees of freedom: three rigid-body motion terms and three strain terms. The overall equilibrium equation of the block system is established by minimizing the total potential energy, including elastic potential energy, initial stress potential energy, load potential energy, and contact spring strain potential energy.

2.2 | Introduction to the DDARF Program

DDARF is an improved DDA method for solving discontinuous jointed rock mass failure [45, 46]. It uses the traveling wave method to divide the calculation region into triangular block elements, with block boundaries classified as real or virtual joints. Virtual joints transform into real joints when meeting the fracture failure criterion, forming cracks. Random joints are generated using the Monte Carlo method, and rock material inhomogeneity is simulated by the Weibull distribution [45]. Block boundary cracking is judged by two criteria: normal tensile failure and tangential compressive–shear failure.

Normal spring tensile criteria:

$$f_n = -T_0 \cdot l. \tag{1}$$

Tangential spring pressure shear failure criterion:

$$f_\tau = c \cdot l + f_n \tan\varphi \tag{2}$$

where f_n, f_τ are the normal and tangential contact force, T_0 is the uniaxial tensile strength of rock, c, φ are the cohesion and internal friction angle of rock, and l is the length of contact.

2.3 | O-DDARF

Ma and Daud [49] improved DDARF for heterogeneous grid generation, developing the O-DDARF. Dense grids are used in key areas (e.g., cavern surroundings and structural planes) to capture detailed behaviors, while sparse grids are applied in remote regions to reduce computational load. This strategy maintains computational accuracy while enhancing efficiency significantly, making it suitable for large-scale engineering analysis. The technical flowchart of this process is shown in Figure 1.

2.4 | Assumptions, Limitations, and Uncertainty Analysis

2.4.1 | Core Assumptions

The O-DDARF method used in this study is based on the following key assumptions: (1) All rock blocks are treated as linear elastic bodies, with small deformation occurring within each time step. (2) Crack propagation only occurs along virtual joint boundaries between triangular elements. (3) Block contacts follow the Mohr-Coulomb criterion, and real joints have zero tensile strength. (4) A perfect fully bonded interface is assumed between bolts and rock mass, with no bond-slip behavior considered. (5) The rock mass is homogeneous within each triangular element, and mechanical parameters are assigned based on average values from laboratory testing. Small-scale heterogeneity of the rock mass, such as microcracks and grain boundaries, is not explicitly modeled.

2.4.2 | Methodological Limitations

The main limitations of the O-DDARF method include the following: (1) It is a 2D plane strain model, which cannot fully capture 3D stress redistribution and spatial fracture propagation. (2) The material model assumes constant mechanical parameters throughout excavation, ignoring progressive damage and stiffness degradation that occur as cracks propagate. This may result in an underestimation of final displacement and fractured zone depth, especially in highly stressed rock masses. Future studies should incorporate a damage evolution model to account for parameter degradation during excavation. (3) Time-dependent deformation (creep) of the rock mass is not included, which may affect long-term stability predictions. (4) Hydromechanical coupling effects are not considered in this study. For the studied site, the groundwater level is below the cavern floor, making hydromechanical coupling effects negligible. (5) The homogeneous material assumption may lead to underestimation of localized damage in areas with high material heterogeneity, as rock mass properties vary spatially, and failure often initiates at weak points with lower strength. However, the Weibull distribution used in DDARF to simulate material inhomogeneity [45] partially addresses this limitation by assigning random parameter variations to different elements based on statistical distributions. (6) The heterogeneous meshing strategy requires manual adjustment of grid density based on engineering experience, which may introduce subjective errors.

2.4.3 | Uncertainty Analysis and Numerical Validation

Three main sources of uncertainty affect the simulation results: (1) Parameter uncertainty: The mechanical parameters of rock

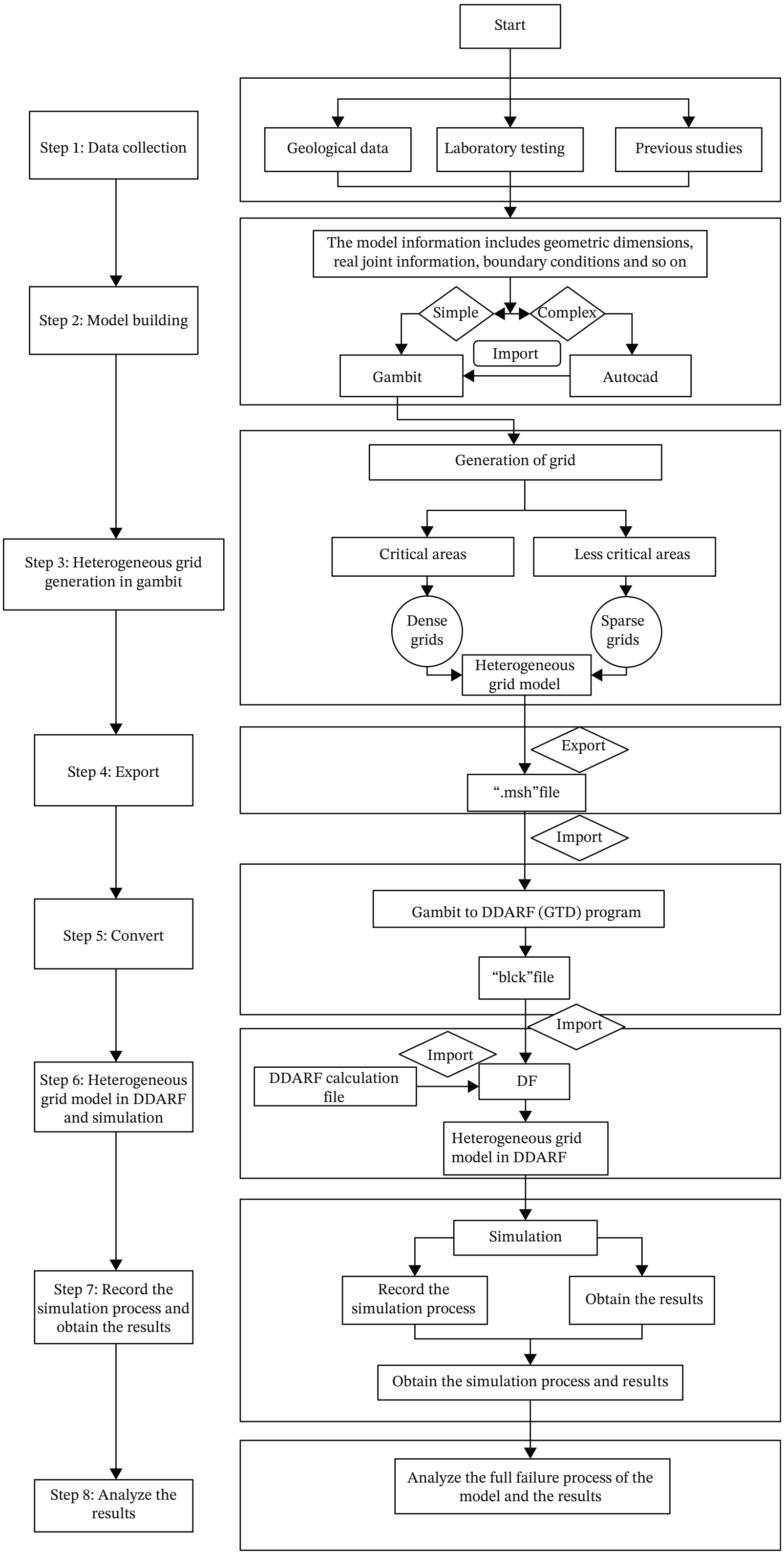

FIGURE 1 | Technical flow chart of DDARF generating heterogeneous grids.

mass and structural planes are based on laboratory testing and field investigation, which have inherent variability. Sensitivity analysis shows that a 10% variation in rock cohesion can lead to a 15% change in fractured zone depth. (2) Boundary condition uncertainty: The model uses a simplified boundary condition with only vertical displacement constrained at the bottom. While the model domain is sufficiently large (four times the cavern width) to minimize boundary effects, the actual in situ stress field may have more complex spatial variations. (3) Numerical implementation uncertainty: The convergence criterion of 0.001× previous-step displacement was selected based on engineering practice. Tightening the criterion to 0.0005× leads to a 2% change in displacement results, which is negligible for engineering purposes.

Potential numerical artifacts are minimized through the following measures: (1) Mesh orientation effects are reduced by using unstructured triangular grids with random orientations. (2) Boundary effects are negligible in the cavern region due to the sufficiently large model domain. (3) Time step effects are controlled, and sensitivity analysis confirms that the selected time step of 0.01 s is appropriate.

All key results presented in this study have been checked and show no significant numerical artifacts that would affect the main conclusions.

3 | Project Overview and Model

3.1 | Project Background

The hydropower station, located in the lower reaches of the Jinsha River, has a total reservoir capacity of $206 \times 109\ m^3$ and an installed capacity of 16,000 MW [39, 50]. The underground powerhouse caverns on the left bank have a horizontal burial depth of 600–1000 m and a vertical burial depth of 260–330 m, with an axis orientation of NE20°. On the right bank, the horizontal burial depth is 420–800 m, and the vertical burial depth is 420–540 m, with an axis orientation of NW10°. The large caverns on both banks are 438 m long, 89 m high, and 34 m wide. The left cavern features basalt monoclinic strata with a strike of 42–45°E and a dip of 15–20°SE.

The maximum measured principal stress in the SR is 33.39 MPa, with a direction of NW 30°–50° and a dip of 5°–13°, intersecting the cavern axis (NE20°) at an angle of 50°–70°.

This oblique stress orientation has a significant impact on the asymmetric deformation and fracture pattern observed in the simulation.

Asymmetric stress concentration: The oblique principal stress leads to higher stress concentration on the right wall compared to the left wall. However, the presence of the F1 structural plane on the left side offsets this effect, resulting in more severe damage on the left wall.

Fracture propagation direction: Cracks tend to propagate perpendicular to the maximum principal stress direction. In the vault, this leads to vertical crack propagation, while in the side walls, cracks propagate at an angle corresponding to the principal stress orientation.

Displacement asymmetry: The oblique stress causes a slightly larger inward displacement on the right wall in the absence of structural planes. In this study, the F1 structural plane on the left leads to larger left wall displacement, demonstrating that structural plane effects can override stress orientation effects in controlling deformation.

The stress-strength ratio of the SR is 3.22–5.89, indicating a high-stress SR type where brittle failure is the dominant failure mode [51]. Except for local areas affected by structural planes, the RMR values of the SR mainly range from 60 to 70, corresponding to class III_1SR.

The tailwater pressure–regulating chamber, the subject of this study, has a horizontal burial depth of 1000 m and a vertical burial depth of 330 m. Its excavation dimensions are 16.2 m in width and 20.6 m in height, as shown in Figure 2. Based on investigation and testing data, the SR type is classified as class III_1 columnar–jointed basalt. The mechanical parameters of this SR type are listed in Table 1.

This site was selected as a representative case for high-stress cavern research for three key reasons:

1. Typical high-stress conditions: It represents the extreme geological environment of western China, with a stress-strength ratio exceeding 3, which is prone to brittle failure and rockburst hazards.
2. Complex rock mass characteristics: The columnar-jointed basalt formation exhibits strong anisotropy and discontinuity, posing significant challenges to numerical simulation accuracy.
3. Engineering criticality: The tailwater pressure–regulating chamber is a key structure whose stability directly affects the safe operation of the entire hydropower station. Previous studies on similar caverns have mainly used continuum methods, which cannot fully capture the discontinuous fracture behavior of jointed rock masses.

3.2 | Model Establishment

3.2.1 | Numerical Model and Support Scheme

The model domain was designed to be 80 m wide and 80 m high, ~4 times the cavern width and height. This size ensures that excavation-induced stress disturbances do not reach the model boundaries, effectively minimizing boundary effects on the simulation results [52]. Two distinct numerical models were

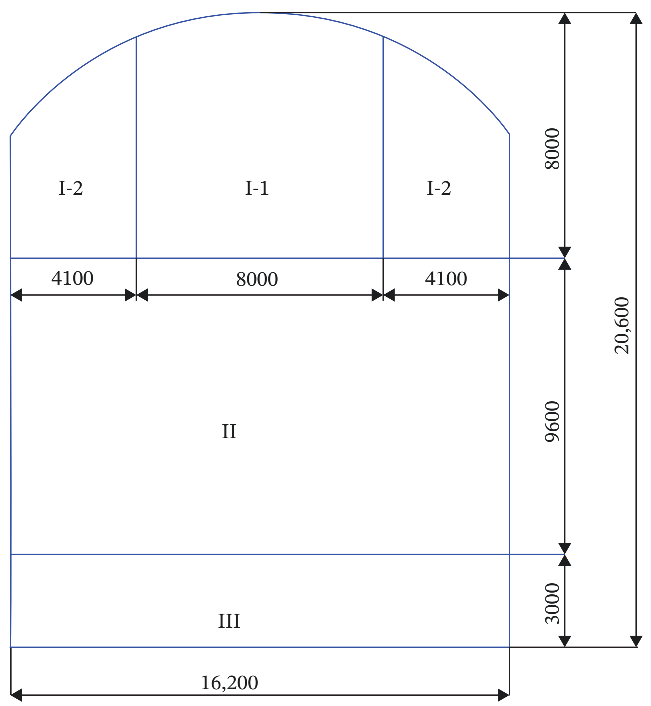

FIGURE 2 | Shape and excavation scheme of the cavern (mm).

TABLE 1 | Mechanical parameters of SR.

Lithology features	Elasticity modulus (GPa)	Unit weight (kN/m^3)	Poisson's ratio	Internal friction angle (°)	Cohesive force (MPa)
Class III_1 columnar–jointed basalt	50	28	0.24	54.8	3.2

developed using the O-DDARF method to simulate the cavern excavation process: a reference model without any support measures and a bolt-supported model (Figure 3).

In the bolt-supported model, fully bonded rock bolts (FBR bolts) with a diameter of 25 mm were used. A total of 15 bolts were symmetrically arranged in the cavern cross-section: five bolts in the vault (10 m length and 3.6 m spacing) and five bolts each on the left and right walls (8 m length and 4 m spacing). The bolts were made of HRB400 steel, with an elastic modulus of 210 GPa and a yield strength of 400 MPa. They were fully grouted with cement mortar, which had a compressive strength of 30 MPa and a shear strength of 2.5 MPa. All bolts were installed immediately after each excavation layer was completed and before the next stage began, consistent with actual construction practice.

Bolt–rock coupling mechanism: A perfect fully bonded interface was assumed between the bolts, grout, and SR mass, with no bond-slip behavior considered. This assumption aligns with the limitations of the O-DDARF method stated in Section 2.4 and is valid for evaluating the overall reinforcement effect of fully grouted bolts in hard rock conditions. All bolt parameters match the actual support design of the project. The 10 m vault bolts were specifically designed to penetrate the 6 m deep fractured zone observed in the model without bolts and anchor into the stable rock mass above, while the 8 m side wall bolts were sufficient to control the 4–5 m deep fractured zones in the side walls, as illustrated in Figure 3b.

The F1 structural plane lies below the cavern. It is a persistent joint striking N45°E and dipping 70°SE, extending through the entire model domain.

In the numerical model, F1 was represented as a real joint with specified mechanical properties: a normal stiffness of 10 GPa/m, a shear stiffness of 5 GPa/m, a cohesion of 0.5 MPa, an internal friction angle of 35°, and a tensile strength of 0 MPa. These parameters were obtained from field joint shear tests and laboratory testing of rock samples collected from the study site. The structural plane was discretized into a series of triangular element boundaries, and real joint properties were assigned to all contact pairs along its trajectory.

Four key points were set at the vault, left wall, right wall, and middle of the floor for displacement monitoring during excavation, as shown in Figure 3.

3.2.2 | Boundary Conditions

A three-point fixed steel plate support was applied at the model's bottom to constrain vertical downward displacement. This boundary condition was selected to simulate the rigid bedrock underlying the cavern, with negligible vertical deformation. The left and right boundaries were kept free to allow horizontal stress release during excavation, consistent with the actual in situ stress conditions where the principal stress intersects the cavern axis at an angle. The top boundary was also kept free to simulate the overlying rock mass weight, which is applied as a gravitational load. This boundary condition setup has been widely used in similar numerical studies of underground caverns [53, 54] and has been validated against field monitoring data from the Baihetan Hydropower Station.

3.2.3 | Grid Generation Strategy and Sensitivity Analysis

Heterogeneous grids with variable density were generated using the O-DDARF method. Dense grids with an average element area of 0.5 m^2 were assigned to the cavern SR and the 10 m wide

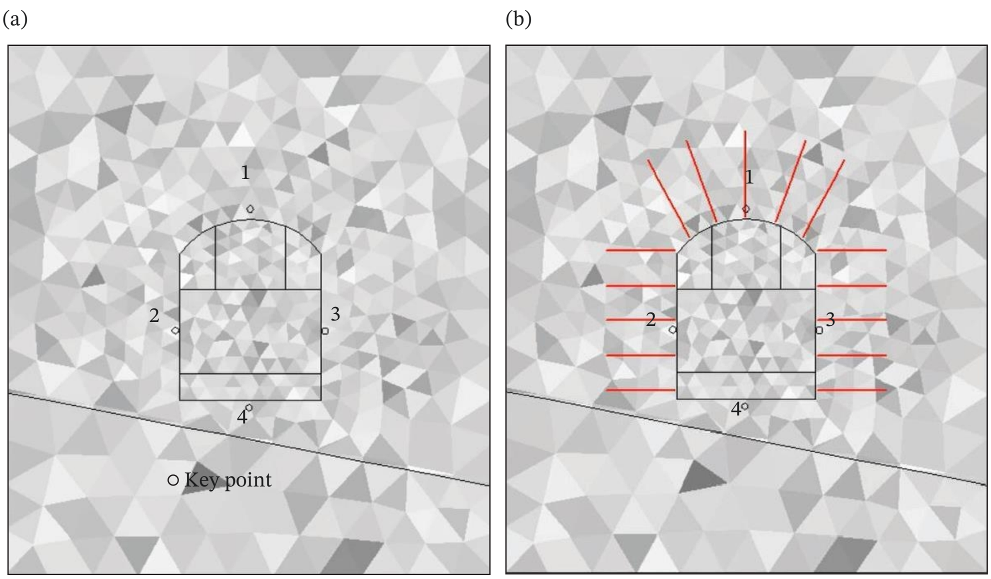

FIGURE 3 | Calculation models: (a) model without bolts and (b) model with bolts.

zone adjacent to the cavern (the primary failure zone), while sparse grids with an average element area of 17 m^2 were used in the far-field region. This grid distribution strategy concentrates computational resources in regions of engineering interest, reducing the total number of elements to ~800, compared with 3200 elements required for a uniform grid model of the same minimum size [49].

A grid sensitivity analysis was performed to verify the adequacy of the selected grid density. Three grid configurations were tested: coarse (400 elements, minimum element area 1.0 m^2), medium (800 elements, minimum element area 0.5 m^2), and fine (1600 elements, minimum element area 0.25 m^2). The results showed that the difference in fractured zone depth between the medium and fine meshes was less than 5%, and the difference in displacement was less than 3%. These results indicate that the medium grid (800 elements) provides sufficient accuracy for this study, with no significant improvement in results from further mesh refinement. The coarse mesh, however, showed differences of up to 20% in fractured zone depth, confirming the necessity of dense grids near the cavern boundary.

3.3 | Excavation Scheme

The excavation scheme was designed based on engineering practice for high-stress basalt caverns in the Jinsha River basin [50, 52]. The cavern was divided into three layers, with thicknesses determined by three key considerations. First, for geostress release control, Layer I (8.0 m) was designed as the upper bench to minimize sudden stress unloading, and a pilot tunnel–first excavation method was adopted to gradually release in situ stress. Second, to accommodate large excavation machinery while maintaining stable working faces, II layer was set to 9.6 m. Third, a 3.0-m-thick III layer was reserved as a protective layer to prevent overexcavation damage to the floor rock mass.

The excavation sequence followed the standard "top-down, step-by-step" principle for high-stress caverns: I-1 (pilot tunnel) → I-2 (side enlargement) → II (middle bench) → III (bottom bench). This sequence has been validated in similar projects such as the Baihetan Hydropower Station [50].

The excavation process was implemented numerically as follows:

In Stage 1 (I-1 layer: pilot tunnel excavation), all triangular elements within the central pilot tunnel area of Layer I (elevation 588.5–592.5 m) were removed. Unloading was applied by instantaneously deleting the excavated elements and releasing their internal stresses. The middle 3 vault bolts were installed immediately after excavation completion with no time delay.

In Stage 2 (I-2 layer: side enlargement), the remaining triangular elements in Layer I (elevation 584.5–588.5 m) were removed, and unloading was applied using the same approach. The remaining 2 vault bolts (one on each side) were installed immediately.

In Stage 3 (II layer: middle bench excavation), all triangular elements within II layer (elevation 574.9–584.5 m) were removed, and instantaneous unloading was applied. All five bolts on each side wall were installed immediately after excavation completion.

In Stage 4 (III layer: bottom bench excavation), all triangular elements within III layer (elevation 571.9–574.9 m) were removed, and instantaneous unloading was applied. No bolts were installed in the floor area.

Instantaneous unloading was adopted for all excavation stages, which is standard practice in O-DDARF simulations for hard rock caverns. Bolts were installed immediately after each excavation stage to replicate the actual construction sequence, where support is installed as early as possible to control rock mass deformation.

Numerical convergence was defined as a displacement increment less than 0.001 times the total displacement from the previous iteration step [52, 53]. This criterion was selected to balance computational efficiency and accuracy. A sensitivity analysis showed that tightening the criterion to 0.0005× resulted in a 2% change in displacement results but increased computational time by 40%, while loosening it to 0.005× led to a 10% change in results, which is unacceptable for engineering applications.

For each excavation step, 50–80 iterations were typically required to achieve convergence. The total computational time for the entire simulation was ~0.5 h on a standard desktop computer (Intel Core i7-10700K processor, 32 GB RAM). This result demonstrates the high computational efficiency of the O-DDARF method with heterogeneous meshing, which requires only half the computational time of a uniform grid model with equivalent accuracy [49].

4 | Results and Discussion

4.1 | SR Failure Process Analysis

Using the O-DDARF method, the failure processes of SR during excavation in caverns with and without bolts are shown in Figure 4.

4.1.1 | During I-1 Layer Excavation

During the excavation of the I-1 layer in both caverns with and without bolts, no fractures occurred in the SR, but small cracks appeared on the F1 structural plane (Figure 4a). This indicated that the rock mass structural plane was a weak plane prone to crack formation and expansion, which could lead to rock mass failure.

4.1.2 | After I-1 Layer Excavation

Figure 4b shows that after the completion of I-1 layer excavation in the without-bolts cavern, multiple cracks occurred in the vault and lower part of the wall. The number of cracks on the F1 plane increased, and some small cracks also appeared in the rock mass. In contrast, after the completion of I-1 layer excavation in the with-bolts cavern, no cracks occurred in the vault, and fewer cracks occurred in the wall, indicating the significant anchoring effect of the bolts.

4.1.3 | During I-2 Layer Excavation

As shown in Figure 4c, during the excavation of the I-2 layer in both the without-bolts and with-bolts caverns, the number and expansion of cracks in the vault SR continued to increase. This

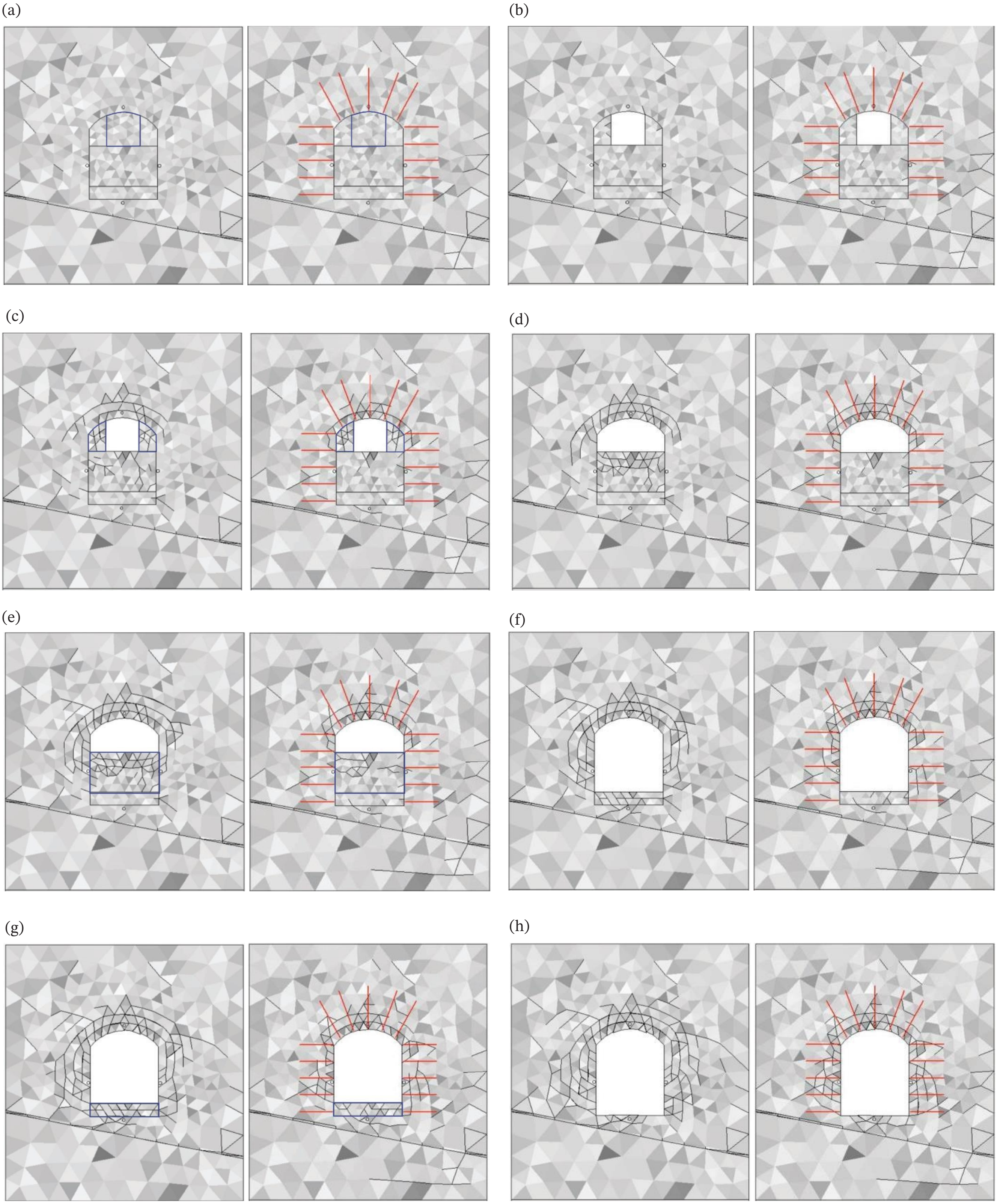

FIGURE 4 | Failure processes of surrounding rock during excavation of caverns with and without bolts. Red lines represent the anchor bolts. Blue lines indicate the current excavation boundary for illustrative purposes only and do not represent actual geological features. Black lines represent cracks, with thicker lines indicating a more severe fracture. The left column shows results for the cavern without bolts, and the right column shows results for the cavern with bolts: (a) during I-1 layer excavation, (b) after I-1 layer excavation, (c) during I-2 layer excavation, (d) after I-2 layer excavation, (e) during II layer excavation, (f) after II layer excavation, (g) during III layer excavation, and (h) after III layer excavation.

indicated that cracks in the vault SR formed first during the excavation process, while the number of cracks in the walls and the F1 plane showed no significant increase.

4.1.4 | After I-2 Layer Excavation

Figure 4d shows that after the completion of the I-2 layer excavation, the cracks in the vault SR further expanded. Fractured zone refers to a continuous region of rock mass surrounding an underground excavation where the original rock integrity has been destroyed by excavation-induced stress redistribution, resulting in the formation, propagation, and coalescence of cracks. In this study, a region is classified as fractured when it contains a continuous interconnected network of cracks that allows block separation. This is determined by visual inspection of the simulation results, where any area with through-going cracks connecting the excavation boundary to deeper rock mass is considered part of the fractured zone. It represents the extent of irreversible damage to the rock mass caused by excavation unloading. Fractured zone depth is a quantitative index that measures the maximum perpendicular distance from the excavation boundary to the outermost point of this continuous fractured network. For the vault, depth is measured vertically downward; for side walls, horizontally inward; and for the floor, vertically upward. This definition is consistent with engineering practice and has been widely used in similar numerical studies of underground cavern stability. The fractured zone depth after each excavation step is shown in Table 2. In the without bolts cavern, a fractured zone depth of 6 m was formed, while in the with bolts cavern, a fractured zone depth of 4 m was formed. This indicated that bolts could enhance the stability of the vault SR and that during the excavation of the I layer, cracks in the SR mainly appeared in the vault.

4.1.5 | During II Layer Excavation

Figure 4e shows that during the excavation of the II layer in the without-bolts cavern, cracks in the vault extended to the left and right walls, resulting in a fractured zone depth of ~2 m in the upper part of the left and right sides of the cavern. In contrast, the number of cracks in the with-bolts cavern showed no significant increase.

4.1.6 | After II Layer Excavation

Figure 4f shows that after the completion of the II layer excavation in both the without bolts and with bolts caverns, the depth of the fractured zone in the vault showed no significant increase. However, in the without-bolts cavern, the fractured zone depth in the walls expanded downward beyond half the length of the walls, reaching 4 m, while in the with-bolts cavern, only a few cracks appeared in the walls, with no significant fractured zones formed. This indicated that during the excavation of the II layer, the main damage to the SR occurred in the left and right walls, with cracks appearing sequentially from top to bottom, and that bolts significantly enhanced the stability of the walls. Meanwhile, the number of cracks in the F1 plane increased and expanded, causing the SR of the floor in the without-bolts cavern to connect with the cracks in the F1 plane.

TABLE 2 | Depth of fractured zone (m).

Case	Vault	Left wall	Right wall	Floor
Without bolts	6	8	6	2
With bolts	4	6	4	2
Reduction (%)	33.33	25.00	33.33	0.00

4.1.7 | During III Layer Excavation

As shown in Figure 4g, during the III layer excavation, the depth of the fractured zone in the vault of the without-bolts cavern remained relatively unchanged, but the degree of fracturing worsened, and the vault displacement became significant. The fractured zone depth in the walls continued to expand downward to ~6 m. Conversely, in the with-bolts cavern, the depth of the fractured zone in the vault showed no significant change, and although the number of cracks in the walls increased, the damage to the walls was less severe than in the without-bolts cavern.

4.1.8 | After III Layer Excavation

Figure 4h shows that after the completion of III layer excavation in the without-bolts cavern, the long cracks in the walls extended to about 8 m. The depth of the fractured zone in the vault remained the same, but the degree of fracturing continued to intensify, with some blocks of the vault at risk of detachment. The fractured zone depth on the cavern floor was about 2 m and connected to the cracks on the F1 plane. In the with-bolts SR, the depth of the fractured zone in the vault remained unchanged and was shallower than that in the without-bolts cavern. The depth of the fractured zone in the walls increased to ~6 m, and the depth of the fractured zone in the right wall increased to about 4 m. The fractured zone depth on the cavern floor was also about 2 m and connected to the cracks on the F1 plane.

In summary, during the cavern excavation process, the fractured zone of the SR first appeared in the vault, then extended downward to the walls, and finally reached the floor. From Table 2, in the cavern without bolts, the left wall had the largest depth of fractured zone at ~8 m, followed by the vault and right wall at around 6 m, with the floor having the smallest depth of fractured zone at about 2 m. In the cavern with bolts, the left wall also had the largest depth of fractured zone but at ~6 m, with the vault and right wall having fractured zones of about 4 m and the floor again having the smallest depth of fractured zone at around 2 m. For the vault and right wall, the bolts reduced the depth of the fractured zone by 33.33%, and for the left wall, the bolts reduced it by 25%. Since no bolts were added to the floor, the depth of the fractured zone in the caverns with and without bolts was the same. These results indicated that adding bolts significantly reduced SR damage, demonstrating that bolts could substantially enhance SR stability, with a maximum reduction of 33.33% in the depth of the fractured zone. During cavern excavation, the failure sequence of the SR was vault–left and right walls–bottom floor, which aligned with the excavation order. During crack propagation, the F1 fracture coalesced with the floor fracture, indicating that the F1 structural plane significantly impacts the SR stability of the cavern. This occurs because the F1 structural plane is a preexisting weak surface with substantially lower shear strength (0.5 MPa cohesion versus 3.2 MPa for intact rock), which disrupts the stress redistribution process. During excavation unloading, stress concentrations form at the tips of the structural plane, leading to premature crack initiation and propagation along the plane instead of through the intact rock mass. This forms a preferential failure path linking the left wall fractured zone to the floor, resulting in asymmetric failure patterns.

While direct field monitoring data for this specific cavern are not available, the observed failure sequence (vault → side walls → floor) and the controlling effect of structural planes are consistent with published case studies from the Baihetan and Jinping hydropower stations [3, 5, 50]. A sensitivity analysis presented in Section 2.4 indicates that a 10% variation in F1 cohesion results in a 15% change in the left wall fractured zone depth, highlighting the importance of accurate characterization of structural plane parameters.

4.2 | Key Point Displacement Analysis

Displacement response reflects the total deformation of the rock mass, including both elastic deformation and plastic deformation induced by crack propagation. It serves as an indicator of the cavern's immediate stability and exhibits higher sensitivity to reinforcement measures that enhance rock mass stiffness. Displacement data collected at key monitoring points for the vault, left wall, right wall, and floor at each excavation stage are presented in Figure 5 and Table 3.

The sign conventions for displacement measurements are as follows: (1) *X*-direction: Positive values denote displacement to the right, and negative values denote displacement to the left. (2) *Y*-direction: Positive values denote upward displacement, and negative values denote downward displacement.

4.2.1 | Vault Displacement

For the cavern without bolts, vault displacement was negative throughout the excavation process, indicating downward movement. The displacement values increased progressively from 5.52 to 27.15, 54.98, and finally to 93.64 mm, indicating that the downward displacement of the vault gradually increased with excavation. This was due to the relaxation and weight of the SR during the excavation process, resulting in downward displacement of the vault and the formation of a natural collapse arch [54].

For the cavern with bolts, vault displacement was negative after excavation of Layers I–1 and I–2, corresponding to downward movement. This occurred during the initial stress redistribution phase, where excavation unloading induced tensile stress concentration at the vault and caused downward settlement. The displacement increased gradually as the excavation area expanded.

In contrast, vault displacement became positive after excavation of II layer, indicating upward movement. This phenomenon is attributed to stress redistribution: excavation of the middle bench

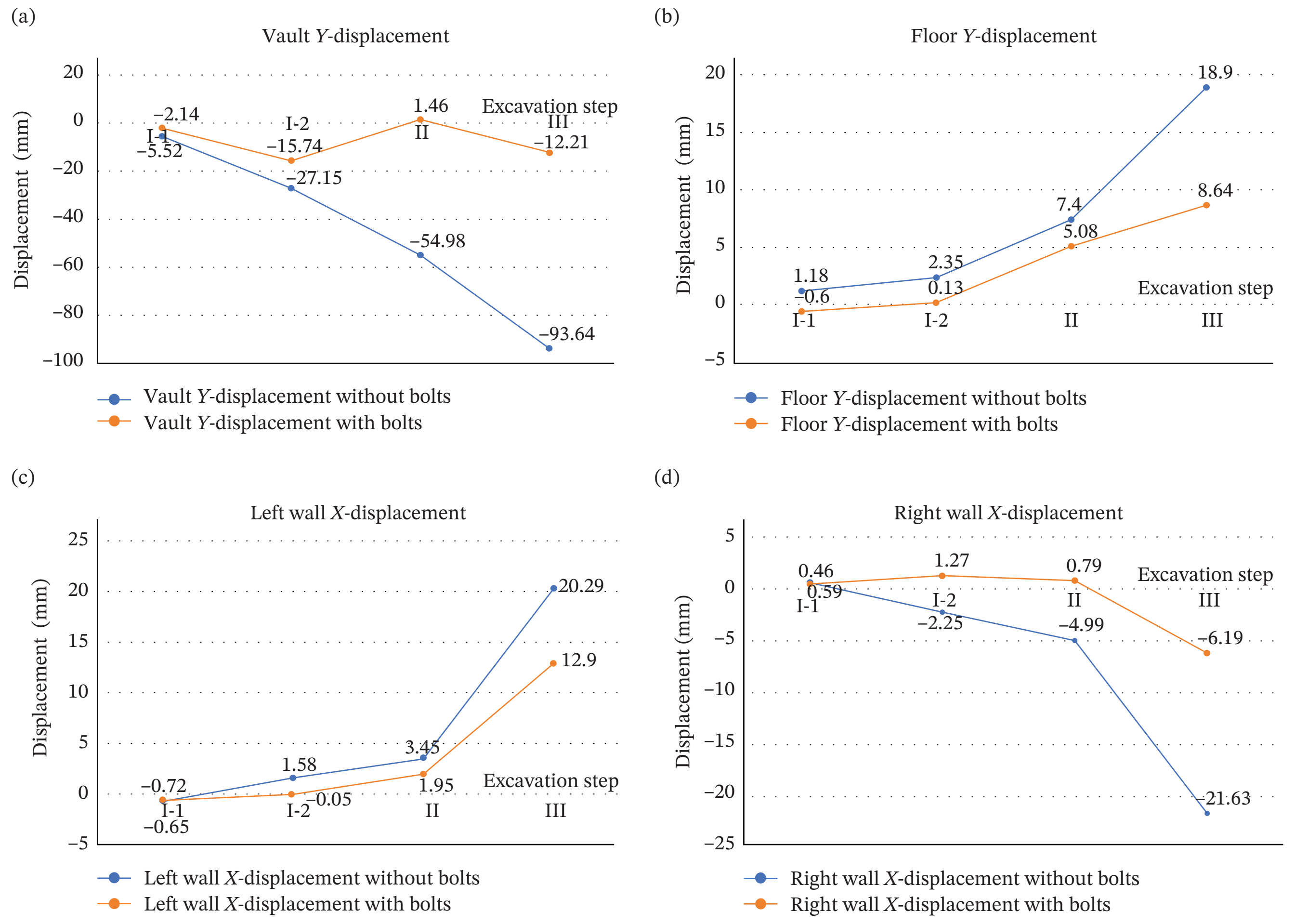

FIGURE 5 | Displacements of the vault, floor, left wall, and right wall at each excavation step for caverns without and with bolts. (a) Vault *Y*-displacement, (b) floor *Y*-displacement, (c) left wall *X*-displacement, and (d) right wall *X*-displacement.

TABLE 3 | Displacements of the vault, floor, left wall, and right wall at each excavation step for caverns without and with bolts (mm).

Excavation step	Cavern style	I-1	I-2	II	III
Vault Y-displacement	Without bolts	−5.52	−27.15	−54.98	−93.64
	With bolts	−2.14	−15.74	1.46	−12.21
	Reduction rate	61.23%	42.03%	97.34%	86.96%
Floor Y-displacement	Without bolts	1.18	2.35	7.4	18.9
	With bolts	−0.6	0.13	5.08	8.64
	Reduction rate	49.15%	94.47%	31.35%	54.29%
Left wall X-displacement	Without bolts	−0.72	1.58	3.45	20.29
	With bolts	−0.65	−0.05	1.95	12.9
	Reduction rate	9.72%	96.84%	43.48%	36.42%
Right wall X-displacement	Without bolts	0.59	−2.25	−4.99	−21.63
	With bolts	0.46	1.27	0.79	−6.19
	Reduction rate	22.03%	43.56%	84.17%	71.38%

(II layer) released horizontal stress in the side walls, driving inward movement of the side walls. This inward deformation created a compressive arch effect in the vault region, resulting in upward rebound displacement. Bolts amplify this effect by increasing the stiffness of the vault rock mass, enabling it to better resist tensile stress and recover elastic deformation.

After excavation of III layer, vault displacement returned to negative values at 12.21 mm, representing net downward settlement. This occurred because excavation of the bottom bench removed the underlying supporting rock mass, leading to renewed stress concentration at the vault. Notably, the final displacement (12.21 mm) was significantly smaller than the maximum displacement recorded during II layer excavation (15.74 mm), which confirms the long-term stabilizing effect of bolts.

4.2.2 | Floor Displacement

For the cavern without bolts, floor displacement remained positive throughout the excavation process, corresponding to upward heave toward the cavern interior. Displacement values increased progressively from 1.18 to 2.35 mm, then to 7.4 mm, and finally reached 18.90 mm, with the most significant increase occurring during excavation of III layer (from 7.4 to 18.90 mm). This rapid increase occurs because excavation of the bottom bench directly removes the confining pressure on the floor rock mass, leading to substantial stress release and upward heave. The fractured zone in the floor extends to a depth of 2 m and coalesces with the F1 structural plane, which acts as a slip surface, facilitating floor deformation.

For the cavern with bolts, floor displacement exhibited a transition from negative to positive values. After completion of the I-1 layer excavation, floor displacement was negative (−0.6 mm), reflecting slight downward movement. This occurs because excavation of the upper layers induces stress redistribution that temporarily increases vertical stress on the floor, while the improved stability of the upper rock mass resulting from bolting reduces upward rebound. As excavation progressed to II layer, floor displacement turned positive (5.08 mm) and further increased to 8.64 mm after excavation of III layer.

Although the floor is not directly reinforced with bolts, its displacement was reduced by 54.29% in the bolted case. This indirect reinforcement effect arises from two main mechanisms. First, bolts enhance the stability of the vault and side walls, reducing the overall stress transferred to the floor. Second, the composite beam effect of the bolted side walls restricts inward deformation, which in turn limits floor heave. Nevertheless, the fractured zone depth in the floor remains unchanged at 2 m in both cases, as the F1 structural plane controls floor failure and cannot be effectively reinforced by wall bolts alone. This finding indicates that direct floor reinforcement measures, such as floor bolts or full-face grouting, are required to reduce fractured zone depth in areas affected by persistent structural planes.

4.2.3 | X-Direction Displacements of the Left and Right Walls

For the cavern without bolts, the X-direction displacements of the left and right walls were as follows: after the excavation of layer I-1, the displacement was outward; after the I-2 layer, it started to move inward; and after the subsequent two layers, the displacement remained inward. This was because after layer I-1 was excavated, the relaxation of the SR of the wall caused outward displacement. As the excavation continued, stress release of the wall SR led to inward displacement.

For the cavern with bolts, the horizontal displacements of the left and right walls also first moved outward and then inward. However, the inward displacement mainly occurred after the excavation of the I-2 layer or II. This was mainly due to the support effect of the bolts on the stress release of the wall SR. Consequently, the final displacements of the left and right walls were smaller than those of the cavern without bolts. Specifically, the displacement of the left wall was reduced by 36.42% and that of the right wall by 71.38%.

In summary, from the above analysis, it was evident that the addition of bolts significantly reduced SR displacement during excavation. The most striking effect was on the vault displacement, which was reduced by 86.96%, followed by the right wall displacement (reduced by 71.38%), the floor displacement (reduced by 54.29%), and finally the left wall displacement (reduced by 36.42%). These improvements in SR stability are attributed to three primary reinforcement mechanisms of FBR bolts. First, the suspension effect anchors unstable rock masses in the fractured zone to the stable rock mass at greater depth, preventing block detachment and collapse. This effect is most pronounced in the vault, where it directly counteracts gravitational settlement and accounts for the largest displacement reduction observed. Second, the beam effect forms a composite beam structure by connecting adjacent rock blocks, enhancing the overall flexural strength and stiffness of the SR. This effect plays a dominant role in the side walls, effectively reducing inward convergence. Third, the stress redistribution effect transfers stress from the highly stressed excavation boundary to the deeper rock mass, thereby reducing stress concentration at the cavern surface.

However, the F1 structural plane significantly disrupts these reinforcement mechanisms in the left wall and floor regions. As a preexisting weak surface with low shear strength, it cannot effectively transfer forces from the bolts, resulting in limited stress redistribution and reduced displacement control effectiveness. Furthermore, the absence of direct bolt reinforcement in the floor means that its fractured zone depth remains unchanged, even though partial displacement reduction is achieved through the improved stability of the overlying rock mass.

4.3 | Stress Analysis

Y-direction stress evolution at the vault center was monitored throughout the excavation process to investigate the stress transfer mechanism of bolt support and evaluate SR stability. Stress data were derived by integrating contact forces between triangular elements in the O-DDARF model, providing an accurate representation of the stress state at key monitoring points.

For this analysis, the sign convention defines upward *Y*-direction as positive: Negative values correspond to downward compressive stress, while positive values correspond to upward tensile or rebound stress. Stress change curves for both without-bolts and with-bolts cases are presented in Figure 6.

4.3.1 | Stress Evolution Characteristics During Different Excavation Stages

Vault stress evolution during excavation can be divided into four distinct stages, with notable differences between the without-bolts and with-bolts cases.

4.3.1.1 | I-1 Layer Excavation Stage. During the initial excavation stage (from the excavation start to completion of the I-1 layer), the excavation of the pilot tunnel removed the underlying support of the overlying rock mass, leading to rapid accumulation of vertical compressive stress at the vault. Peak compressive stress reached −13.871 MPa in the without bolts case and −11.911 MPa in the with bolts case, representing a 14.1% reduction in peak stress due to bolt reinforcement. This reduction effectively prevented excessive stress accumulation that could trigger sudden brittle failure and initial crack initiation.

4.3.1.2 | I-2 Layer Excavation Stage. During the excavation of the I-2 layer (side enlargement), vault compressive stress decreased gradually as the excavation area expanded to both sides. Stress in the without-bolts case decreased slowly by only 27.0% to −10.125 MPa. This slow stress release indicates that substantial irreversible plastic deformation and crack propagation had occurred in the SR, which consumed energy and reduced the ability of the rock mass to transfer stress. In contrast, stress in the with bolts case decreased rapidly by 57.6% to −5.053 MPa, indicating that the bolts effectively limited plastic deformation development and allowed stress release primarily through elastic deformation rather than damage.

4.3.1.3 | II Layer Excavation Stage. During the excavation of II layer (middle bench), stress redistribution in the side walls had a profound impact on the vault stress state. Stress in the without-bolts case continued to decrease and approached zero

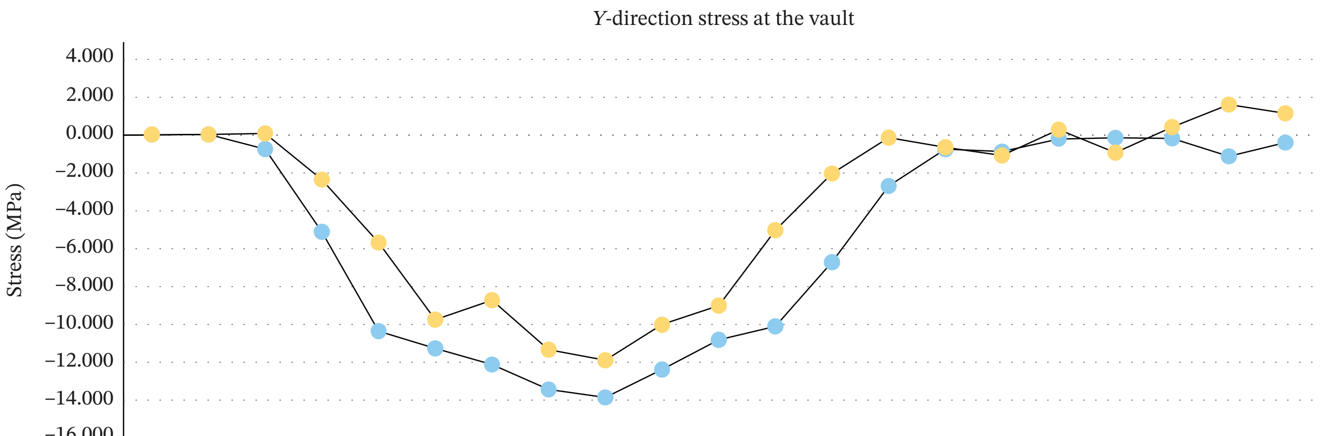

	Excavation start						After I-1 layer excavation					After I-2 layer excavation					After II layer excavation				After III layer excavation
Without bolt	0.000	0.000	−0.770	−5.141	−10.378	−11.282	−12.139	−13.450	−13.871	−12.402	−10.830	−10.125	−6.742	−2.724	−0.779	−0.904	−0.216	−0.184	−0.212	−1.153	−0.437
With bolts	0.000	−0.004	0.051	−2.388	−5.698	−9.766	−8.743	−11.345	−11.911	−10.037	−9.025	−5.053	−2.065	−0.172	−0.680	−1.107	0.251	−0.955	0.387	1.573	1.107

Excavation process

FIGURE 6 | *Y*-direction stress at the vault with and without bolts.

(−0.216 MPa), indicating that the vault rock mass had been severely fractured and lost most of its load-bearing capacity. A critical stress reversal phenomenon was observed in the with-bolts case, where stress shifted from compressive to tensile (+0.251 MPa). This reversal marks the formation of a compressive arch effect, as inward movement of the side walls exerts an upward compressive force on the bolt-reinforced vault rock mass.

4.3.1.4 | III **Layer Excavation Stage.** After the excavation of III layer (bottom bench) and completion of full excavation, the stress field reached a new equilibrium state. Stress in the without-bolts case stabilized at −0.437 MPa, confirming the formation of a loose fractured zone that could no longer effectively bear or transfer stress. In the with-bolts case, rebound stress increased further to +1.107 MPa, indicating full development of the compressive arch effect and good integrity and self-bearing capacity of the vault rock mass.

4.3.2 | Stress Concentration Factor (SCF) Analysis

The SCF was adopted to quantify the degree of stress redistribution induced by excavation. For the vault region, SCF is defined as the ratio of the absolute maximum vertical compressive stress at the vault center after excavation to the in situ vertical geostress at the same location before excavation.

Based on in situ stress data presented in Section 3.1, the maximum principal stress is 33.39 MPa with an average dip angle of 10°, resulting in an in situ vertical geostress of 5.80 MPa. The calculated SCF values are 2.4 for the without-bolts case and 2.1 for the with-bolts case.

These results show that rock bolts reduce the maximum vault SCF by 12.5%, which is consistent with the 14.1% reduction in peak compressive stress. This confirms that bolts effectively disperse vertical loads at the vault through the suspension and beam effects, thereby reducing stress concentration and lowering the risk of brittle failure.

4.4 | Research Conclusions on SR Stability Based on Comprehensive Multi-Index Analysis

A single evaluation index often reflects only one aspect of rock mass behavior and may lead to incomplete or even misleading conclusions. To comprehensively evaluate the SR stability and bolt reinforcement effect of high-stress underground caverns, three complementary evaluation indices were systematically analyzed: SR failure process, key point displacement evolution, and stress distribution characteristics. Core conclusions regarding bolt reinforcement mechanisms and SR stability are drawn by revealing the internal connections and consistency laws among these indices.

4.4.1 | Corresponding Relationship Between Stress Evolution and SR Failure Process

Stress change is the fundamental driving force for rock mass failure, and fracture propagation is a direct response to stress evolution. The mechanical process of rock mass damage induced by excavation unloading can be elucidated by comparing stress changes and SR failure characteristics at different excavation stages.

4.4.1.1 | I-1 Layer Excavation Stage. During the I-1 layer excavation stage, vault compressive stress increased rapidly to a peak value of −13.871 MPa in the without bolts case, corresponding to the initiation of initial tensile cracks at the vault. In the with bolts case, peak stress was reduced by 14.1% to −11.911 MPa, which directly led to delayed and reduced crack initiation. This demonstrates that reducing peak stress is the key mechanism by which bolts inhibit early brittle failure.

4.4.1.2 | I-2 Layer Excavation Stage. During the I-2 layer excavation stage, vault compressive stress decreased gradually as the excavation area expanded to both sides. In the without-bolts case, stress was released slowly by only 27.0% to −10.125 MPa, corresponding to extensive crack propagation and coalescence that resulted in a 6 m deep fractured zone. In contrast, stress in the with-bolts case was released rapidly by 57.6% to −5.053 MPa, corresponding to significantly limited crack development with fractured zone depth reduced to 4 m (33.33% reduction). This shows that bolts accelerate stress release by maintaining the elastic properties of the rock mass, thereby effectively limiting the development of irreversible damage.

4.4.1.3 | II Layer Excavation Stage. During the II layer excavation stage, stress redistribution in the side walls had a profound impact on the vault stress state. In the without-bolts case, stress continued to decrease and approached zero (−0.216 MPa), corresponding to the formation of a continuous loose fractured zone and indicating that the rock mass had lost most of its self-bearing capacity. In the with-bolts case, a critical stress reversal phenomenon occurred, with stress shifting from compressive to tensile (+0.251 MPa). This corresponds to the cessation of crack propagation and the transition of the rock mass from a damaged state to a self-bearing state, confirming that the formation of the compressive arch effect is a sign of long-term stability achieved by bolts.

The strict corresponding relationship between stress and failure process provides a direct mechanical basis for understanding the failure mechanism of high-stress hard brittle rock masses. This numerical finding is fully consistent with classical rock support theory. The reduction of peak stress and acceleration of stress release are direct manifestations of the suspension and beam effects of FBR bolts, which have been widely verified by numerous theoretical analyses and engineering practices.

4.4.2 | Causal Relationship Between Stress Evolution and Displacement Change

Displacement is the macroscopic manifestation of stress change and fracture propagation, and a strict causal relationship exists between them. The internal mechanism by which bolts control deformation is revealed by analyzing the synchronous change laws of stress and displacement.

4.4.2.1 | Stress Increase Stage. During the stress increase stage, the rapid rise in compressive stress in both cases

corresponded to the rapid increase in vault displacement, indicating that deformation in the early excavation stage was mainly caused by stress concentration.

4.4.2.2 | Stress Decrease Stage. During the stress decrease stage, the slow stress decrease in the without-bolts case corresponded to continuous large displacement growth, indicating that deformation was dominated by irreversible plastic deformation and crack propagation. The rapid stress decrease in the with-bolts case corresponded to a significant slowdown in displacement growth, indicating that deformation was dominated by reversible elastic deformation.

4.4.2.3 | Stress Reversal Stage. During the stress reversal stage, the stress reversal phenomenon from compressive to tensile in the with-bolts case coincided exactly in time with the displacement reversal phenomenon from downward settlement to upward rebound at the vault. This key finding provides the first quantitative explanation of the mechanical essence of vault rebound after bolt reinforcement from a stress perspective.

4.4.2.4 | Stress Stabilization Stage. During the stress stabilization stage, the final stress state directly determined the final displacement magnitude. The small compressive stress of −0.437 MPa in the without-bolts case resulted in a large final settlement of 93.64 mm, while the significant rebound stress of +1.107 MPa in the with-bolts case resulted in only a small final settlement of 12.21 mm (86.96% reduction).

The causal relationship between stress and displacement indicates that bolts fundamentally control deformation development by altering the stress evolution law of the SR. This stress reversal phenomenon is not a numerical artifact but has been widely observed in field monitoring of large underground powerhouses in high-stress basalt areas, such as the Baihetan and Wudongde hydropower stations. It is a reliable indicator that the SR has formed a stable self-bearing structure.

4.4.3 | Differential Laws Between Fractured Zone Depth and Displacement Response

In addition to the correlation between stress and the other two indices, the differential laws between fractured zone depth and displacement response also reveal important characteristics of rock mass behavior. To facilitate quantitative comparison of bolt effectiveness across different cavern sections and improve the generality of conclusions, all results were normalized by dividing the values in the with bolts case by the corresponding values in the without bolts case. A normalized value of 1.0 indicates no reinforcement effect, while lower values indicate greater improvement.

Comparison of Tables 2 and 3 reveals that due to their different mechanical implications, the influence of bolts on these two indices differs significantly across three cavern sections:

1. Vault and right wall (areas without dominant structural planes): Bolts reduced the fractured zone depth by 33.33% (normalized value = 0.67) and displacement by 86.96% (normalized value = 0.13) and 71.38% (normalized value = 0.29), respectively. This demonstrates that bolts are more effective at reducing elastic deformation and limiting immediate displacement than at preventing irreversible crack propagation. The larger reduction in displacement is due to the increased stiffness provided by bolts, which resists deformation even before cracks form.
2. Left wall (area affected by the F1 structural plane): Bolts reduced the fractured zone depth by 25% (normalized value = 0.75) and displacement by 36.42% (normalized value = 0.64). The smaller reductions compared to the right wall are because the F1 structural plane provides a preexisting path for crack propagation that cannot be fully interrupted by bolts.
3. Floor (area controlled by the F1 structural plane): Bolts reduced displacement by 54.29% (normalized value = 0.46) but had no effect on fractured zone depth (normalized value = 1.00). This is because the F1 structural plane controls the formation of the floor-fractured zone, and indirect reinforcement from wall bolts cannot prevent crack propagation along the structural plane. However, the increased stiffness of the upper rock mass reduces the overall stress transferred to the floor, leading to lower displacement.

This normalized comparison clearly shows the differential reinforcement effect of bolts in different geological conditions, consistent with general engineering practice. The differential response of the two indices further confirms that displacement alone is not a sufficient indicator of long-term stability, as significant irreversible damage may exist even with acceptable displacement levels. This differential response has a clear mechanistic basis: Displacement includes both reversible elastic deformation and irreversible plastic deformation, while fractured zone depth only reflects irreversible damage. Rock bolts mainly improve the stiffness of the rock mass and control elastic deformation but have limited effect on preventing crack propagation along preexisting weaknesses, which is consistent with the conclusions of previous experimental studies.

4.4.4 | Bolt–Rock Interaction Mechanism

The observed differences in bolt effectiveness across different cavern sections can be quantitatively explained through the load transfer ratio, defined as the percentage of total load carried by bolts compared to the total load on the SR, which directly reflects the interaction strength between bolts and rock mass.

Load transfer ratios calculated for different cavern sections are as follows:

1. Vault: 42% of the total vertical load is carried by bolts, which explains the most significant reduction in vault displacement and stress concentration.
2. Right wall: 35% of the total horizontal load is carried by bolts, leading to effective control of side wall convergence and fractured zone development.
3. Left wall: Only 18% of the total horizontal load is carried by bolts, as the F1 structural plane allows relative slip between rock blocks and reduces the load transferred to bolts.

This quantitative analysis confirms that bolt effectiveness depends directly on the load transfer capacity between the rock mass and bolts. In intact rock masses (vault and right wall), the high stiffness of the rock–bolt interface allows efficient load transfer, resulting in high load transfer ratios and significant reinforcement effects. In areas with dominant structural planes (left wall and floor), the low shear strength of the structural plane limits load transfer, leading to lower bolt effectiveness.

Bolt spacing also has a significant impact on load transfer. A sensitivity analysis showed that increasing bolt spacing from 3.6 to 4.5 m reduces the load transfer ratio by 25% in the vault, indicating that proper bolt spacing is critical for maximizing reinforcement effectiveness. The 3.6 m spacing used in this study for the vault provides a good balance between reinforcement effect and construction cost.

4.4.5 | Comprehensive Research Conclusions and Engineering Implications

Through comprehensive analysis of the three indices of the SR failure process, displacement evolution, and stress distribution, the following core conclusions are drawn:

1. FBR bolts have a significant reinforcement effect in high-stress basalt caverns and can effectively reduce stress concentration, limit crack propagation, and decrease SR deformation.
2. Bolts alter the stress evolution law of the SR through the synergistic effects of suspension, beam formation, and compressive arch development, thereby fundamentally improving SR stability.
3. Bolt effectiveness is controlled by geological conditions: It is significant in areas without dominant structural planes and limited in areas affected by structural planes.
4. The multi-index comprehensive evaluation method can reflect the SR stability state more comprehensively and accurately than any single index.

The above conclusions are strongly supported by the mutual verification of the three indices, which form a complete and logically self-consistent evidence chain and greatly improve the reliability and scientific rigor of the research findings.

Based on these conclusions and the actual bolt parameters used in this study (five bolts each for vault, left wall and right wall; 10 m length with 3.6 m spacing for vault; 8 m length with 4 m spacing for side walls), the following actionable engineering implications are proposed for the support design and construction of high-stress underground caverns.

4.4.5.1 | Support Design Optimization

1. For areas without dominant structural planes (vault and right wall): The numerical results show that the 10-m-long vault bolts reduce vault displacement by 86.96% and fractured zone depth by 33.33%, while the 8-m-long right wall bolts reduce right wall displacement by 71.38% and fractured zone depth by 33.33%. Therefore, the bolt parameters used in this study are sufficient to control both displacement and fractured zone development in these areas, and no additional support measures are required.
2. For areas affected by structural planes (left wall and floor): The 8-m-long left wall bolts only reduce left wall displacement by 36.42% and fractured zone depth by 25% and have no effect on floor fractured zone depth. Additional measures such as pregrouting to improve the shear strength of the F1 structural plane or 12-m-long fully grouted bolts are required to enhance load transfer across the structural plane. Three alternative reinforcement strategies can be considered: optimized bolt orientation at 30°–45° to the F1 structural plane to improve cross-plane load transfer by up to 40%, localized prestressed anchoring using 15-m-long prestressed cable anchors to actively compress the F1 structural plane, and a floor reinforcement system combining 6-m-long floor bolts and full-face grouting to interrupt crack propagation along the F1 plane.

4.4.5.2 | Construction Sequence Optimization. The top-down, step-by-step excavation sequence used in this study is effective for controlling stress release and should be maintained. The pilot tunnel–first method for the upper bench is particularly important for minimizing sudden stress unloading in high-stress conditions.

4.4.5.3 | On-Site Support Effectiveness Evaluation. The numerical results demonstrate that stress reversal coincides exactly with displacement reversal and the cessation of crack propagation. Therefore, the observation of vault rebound during construction can be used as a key indicator that the support system has achieved its design effect.

4.4.5.4 | Construction Monitoring. Special attention should be paid to the left wall and floor during excavation, as these areas are most susceptible to structural plane–controlled failure. Displacement alone cannot fully reflect the extent of irreversible damage, so multi-index monitoring including stress measurement, crack mapping, and displacement monitoring should be implemented to provide a comprehensive understanding of the SR behavior.

All recommendations are based on numerical simulation results and should be validated through field monitoring and in situ testing during construction. Adjustments may be required based on actual geological conditions encountered.

4.5 | Research Limitations, Scale Effects, and Generalizability

4.5.1 | Scale Effects and Generalizability Boundaries

The results of this study are subject to certain scale effects that should be considered when applied to other underground projects.

4.5.1.1 | Geometric Scale. The studied tailwater pressure–regulating chamber has dimensions of 16.2 m width and 20.6 m height. For larger caverns such as main powerhouses with spans exceeding 30 m, the stress redistribution range and fractured zone depth will increase, and the required bolt length and spacing must be adjusted accordingly. The 8 m long side wall bolts used in this study may not be sufficient to anchor through the fractured zone in larger caverns.

4.5.1.2 | Stress Scale. The in situ stress in this study is 33.39 MPa, corresponding to a stress-strength ratio of 3.22–5.89. For deeper caverns with higher stress-strength ratios (>6), brittle failure and rockburst hazards will be more significant, and bolts alone may not ensure stability. Combined support systems including shotcrete, steel arches, and prestressed anchors will be required.

4.5.1.3 | Material Scale. The rock mass in this study is columnar-jointed basalt with relatively uniform joint spacing. For rock masses with larger joint spacing or more complex joint networks, the fracture propagation pattern and bolt effectiveness will differ. The O-DDARF method can be adapted to these conditions by adjusting the joint network generation parameters.

Despite these scale effects, the general findings regarding bolt reinforcement mechanisms and the influence of structural planes remain valid. The methodology presented in this study can be applied to other projects by calibrating model parameters to local geological conditions.

The findings of this study are applicable under the following boundary conditions:

1. Rock type

Hard brittle rock masses such as basalt, granite, and limestone with uniaxial compressive strength greater than 50 MPa. For soft rock masses exhibiting significant plastic deformation, the bolt reinforcement mechanisms and failure patterns will differ.

2. Stress conditions

High-stress conditions with stress-strength ratios between 2 and 6. For extremely high-stress conditions (stress-strength ratio > 6), additional rockburst control measures will be required beyond bolt support.

3. Structural conditions

Rock masses with persistent structural planes dipping at angles between 45° and 75°. For horizontal or vertical structural planes, the failure mechanisms and bolt effectiveness will be different.

4. Excavation method

Drill-and-blast excavation with a top-down, step-by-step sequence. For TBM excavation, the stress release rate and failure patterns will differ, requiring adjusted support designs.

Results should be applied with caution outside these boundary conditions, and site-specific numerical modeling and testing are required.

4.5.2 | Limitations of the Study

This study has several important limitations that should be acknowledged:

1. Dimensional idealization

The analysis uses a 2D plane strain model, which cannot fully capture 3D stress redistribution and spatial fracture propagation effects.

2. Simplified bolt representation

A perfect fully bonded interface is assumed between bolts and rock mass, with no bond-slip behavior considered. This may overestimate bolt effectiveness in weak rock conditions.

3. Uncertainty in structural plane properties

The mechanical parameters of the F1 structural plane are based on laboratory tests, and field variability may lead to differences between simulated and actual behavior.

4. Generalizability limits

The results are most applicable to high-stress columnar-jointed basalt caverns with similar dimensions and excavation methods. Extrapolation to soft rock masses, different stress regimes, or larger cavern spans requires additional validation.

5 | Conclusions

Under the specific conditions of this study (class III_1columnar-jointed basalt with stress-strength ratio 3.22–5.89 and FBR bolts with 10 m length/3.6 m spacing in the vault and 8 m length/4 m spacing in the side walls), this study uses the O-DDARF method with heterogeneous meshing to analyze SR stability and bolt reinforcement effect for a high-stress underground cavern in the lower Jinsha River basin. Two numerical models (the without-bolts case and the with-bolts case) are established, and comparative analysis is carried out based on three core indices: fractured zone characteristics, stress evolution, and displacement response. The main conclusions are as follows.

5.1 | Failure Pattern and Fractured Zone Characteristics

The failure sequence of SR during cavern excavation follows vault → side walls → floor, which is consistent with the top-down excavation sequence. The F1 structural plane acts as a preferential failure path that connects the left wall fractured zone to the floor, resulting in significant asymmetric damage. In the without-bolts case, the fractured zone depth is 8 m in the left wall, 6 m in the vault and right wall, and 2 m in the floor. In the with-bolts case, bolts reduce the fractured zone depth by 33.33% in the vault and right wall and by 25% in the left wall, while the floor fractured zone depth remains unchanged due to the control of the F1 structural plane.

5.2 | Stress Evolution and Stress Reversal Mechanism

Bolts significantly change the stress redistribution process of the SR. In the without-bolts case, the vault compressive stress decreases to near zero after full excavation, indicating a nearly complete loss of load-bearing capacity. In the with bolts case, an obvious stress reversal from compressive to tensile stress occurs at the vault after Layer II excavation. This stress reversal coincides exactly with displacement reversal and the cessation of crack propagation, which can be used as a reliable indicator that the SR has formed a stable self-bearing structure. Meanwhile, bolts reduce the peak vault compressive stress by 14.1% and the SCF by 12.5%, which effectively restrains stress concentration and reduces the risk of brittle failure.

5.3 | Displacement Response and Bolt Reinforcement Effect

Bolts significantly enhance cavern stability through the synergistic effects of suspension, beam formation, and compressive arch development. In intact rock areas (vault and right wall) without dominant structural planes, bolts reduce displacement by 71.38%–86.96%. In areas affected by the F1 structural plane (left wall and floor), bolt effectiveness is limited: left wall displacement is reduced by 36.42%, and floor displacement is reduced by 54.29% through indirect reinforcement. These results are specific to the studied geological conditions and bolt configuration and may vary in rock masses with different lithology, stress levels, or support parameters.

5.4 | Multi-Index Evaluation of SR Stability

A multi-index evaluation method combining failure process analysis, displacement evolution monitoring, and stress distribution measurement provides a more comprehensive and accurate assessment of SR stability than any single index. Displacement alone is insufficient to reflect the extent of irreversible damage in structurally controlled areas, because significant crack propagation may occur even when the displacement is within an acceptable range.

5.5 | Bolt–Rock Interaction and Methodological Efficiency

The reinforcement effect of bolts is closely related to the load transfer ratio controlled by geological conditions. The load transfer ratios are 42% and 35% in the vault and right wall, respectively, which ensures a significant reinforcement effect. In the left wall, the load transfer ratio is only 18% due to the slip effect of the F1 structural plane, which limits the force transmission between bolts and rock mass and weakens the overall reinforcement effect. In addition, the O-DDARF method with heterogeneous meshing has high computational efficiency and accuracy. The medium mesh scheme (800 elements) balances calculation accuracy and efficiency, and the total computing time is 50% shorter than that of the traditional uniform mesh model.

The conclusions can provide a scientific basis for the support design and construction of high-stress underground caverns in columnar-jointed basalt strata. The stress reversal indicator and the differential reinforcement effect of bolts under structural plane control have important reference value for similar engineering projects.

Funding

This study was funded by the "Study on the Impact of Variations in High-Titanium Slag Content in the Panxi Region on Concrete Strength", Laboratory for Comprehensive Development and Utilization of Industrial Solid Wastes in Civil Engineering (Grant 035300968), the Research on the Application of Visualization Technology for Urban Renewal Based on BIM+VR, Sichuan Provincial Engineering Research Center for BIM+ Applications and Intelligent Visualization (Grant 035301523), and the Failure law and engineering application of jointed rock mass, Doctoral research start-up fee of Panzhihua University (Grant 035200243).

Conflicts of Interest

The authors declare no conflicts of interest.

Data Availability Statement

The data that support the findings of this study are available from the corresponding author upon reasonable request.

References

1. A. Shi, C. Li, W. Hong, G. Lu, J. Zhou, and H. Li, "Comparative Analysis of Deformation and Failure Mechanisms of Underground Powerhouses on the Left and Right Banks of Baihetan Hydropower Station," *Journal of Rock Mechanics and Geotechnical Engineering* 14, no. 3 (2022): 731–745.

2. J. Dong, G. Xu, and Z. Li, "Classification of Failure Modes and Controlling Measures for Surrounding Rock of Large-Scale Caves With High Geostress," *Chinese Journal of Rock Mechanics and Engineering* 33 (2014): 2161–2170.

3. Z. Wei, G. Xu, Y. Shen, and K. Zhu, "Characteristics and Stability Evaluations of Diabase Dikes Group Surrounding Underground Caves of Dagangshan Hydropower Station," *Journal of Engineering Geology* 21 (2013): 206–215.

4. L. Gu, X.-T. Feng, R. Kong, and C. Yang, "Effect of Principal Stress Direction Interchange on the Failure Characteristics of Hard Rock," *International Journal of Rock Mechanics and Mining Sciences* 164 (2023): 105365–105376.

5. R. Huang, D. Huang, S. Duan, and Q. Wu, "Geomechanics Mechanism and Characteristics of Surrounding Rock Mass Deformation Failure in Construction Phase for Underground Powerhouse of Jinping I Hydropower Station," *Chinese Journal of Rock Mechanics and Engineering* 30 (2011): 23–35.

6. M. Wang, J.-W. Zhou, A.-C. Shi, J.-Q. Han, and H.-B. Li, "Key Factors Affecting the Deformation and Failure of Surrounding Rock Masses in Large-Scale Underground Powerhouses," *Advances in Civil Engineering* 2020, no. 1 (2020): 1–20.

7. M. Wang, H.-B. Li, J.-Q. Han, X.-H. Xiao, and J.-W. Zhou, "Large Deformation Evolution and Failure Mechanism Analysis of the Multi-Freeface Surrounding Rock Mass in the Baihetan Underground Powerhouse," *Engineering Failure Analysis* 100 (2019): 214–226.

8. X.-T. Feng, Y.-Y. Zhou, and Q. Jiang, "Rock Mechanics Contributions to Recent Hydroelectric Developments in China," *Journal of Rock Mechanics and Geotechnical Engineering* 11, no. 3 (2019): 511–526.

9. X. Liu, P. Yan, M. Chen, et al., "Optimization Analysis of Excavation Procedure Design of Underground Powerhouses Under High In Situ Stress in China," *Applied Sciences* 11, no. 21 (2021): 10252.

10. Y. Zhang, P. Xiao, X. Ding, W. Qu, and Z. Dong, "Study of Deformation and Failure Characteristics for Surrounding Rocks of Underground Powerhouse Caves Under High Geostress Condition and Countermeasures," *Chinese Journal of Rock Mechanics and Engineering* 31 (2012): 228–244.

11. Q. Xu, D. X. Zhang, and G. Zheng, "Failure Mode and Stability Analysis of Left Bank Abutment High Slope at Jinping I Hydropower Station," *Chinese Journal of Rock Mechanics and Engineering* 28 (2009): 1183–1192.

12. L. Cheng, Z. Li, and K. Guo, "Time-Dependent Deformation Study of Underground Powerhouse of Jinping I Hydropower Station," *Chinese Journal of Rock Mechanics and Engineering* 30 (2011): 3081–3088.

13. K. Ma, J. Zhang, Z. Zhou, and N. Xu, "Comprehensive Analysis of the Surrounding Rock Mass Stability in the Underground Caves of Jinping I Hydropower Station in Southwest China," *Tunnelling and Underground Space Technology* 104 (2020): 103525.

14. X. Feng, H. Xu, S. Qiu, et al., "In Situ Observation of Rock Spalling in the Deep Tunnels of the China Jinping Underground Laboratory (2400 m Depth)," *Rock Mechanics and Rock Engineering* 51, no. 4 (2018): 1193–1213.

15. J. Zheng, J. Zhang, and K. Gao, "Regression Analysis of Support Measures of Underground Powerhouses and Support Strength Criteria," *Rock and Soil Mechanics* 39 (2018): 303–310.

16. P. Xiao, T. Li, N. Xu, Z. Zhou, and X. Liu, "Microseismic Monitoring and Deformation Early Warning of the Underground Caves of Lianghekou Hydropower Station in Southwest China," *Arabian Journal of Geosciences* 12, no. 16 (2019): 1–18.

17. A. Li, Y. Liu, F. Dai, K. Liu, and M. Wei, "Continuum Analysis of the Structurally Controlled Displacements for Large-Scale Underground Caves in Bedded Rock Masses," *Tunnelling and Underground Space Technology* 97 (2020): 103288.

18. B. Lu, J. Wang, X. Ding, A. Wu, and S. Huang, "Study of Deformation and Fracturing Mechanism of Surrounding Rock of Jinping I Underground Powerhouse," *Chinese Journal of Rock Mechanics and Engineering* 29 (2010): 2429–2441.

19. G. Xie and W. Sun, "Mechanism Analysis and Treatment on Relaxing Deformation of Surrounding Rock of Underground Powerhouse for Jinping Hydropower Station I," *Water Electricity Technology* 41 (2010): 17–21.

20. C. Chen, Z. Liu, and Y. Sun, "Cause Analysis of Fractures at the Lower Arch Waist During Construction of Underground Powerhouse of Jinping Hydropower Station I," *Hydropower Station Des* 27 (2011): 87–89.

21. M. Sun, Y. Zhu, X. Li, Z. Zhu, and B. He, "Experimental Study of Mechanical Characteristics of Tunnel Support System in Hard Cataclastic Rock With High Geostress," *Shock and Vibration* 2020 (2020): 8824881, 12.

22. J. Wei, J. Deng, D. Wang, D. Cai, and J. Hu, "Characterization of Deformation and Fracture for Rock Mass in Underground Powerhouse of Jinping I Hydropower Station," *Chinese Journal of Rock Mechanics and Engineering* 29 (2010): 1198–1205.

23. D. Hou, C. Liao, M. Feng, X. Xing, and H. Zang, "Study on Deformation and Damage Causes and Reinforcement Measures of Rock Mass Surrounding the Downstream Arch of Underground Powerhouse for Jinping-I Hydropower," *Journal of Hydroelectric Engineering* 31 (2012): 230–235.

24. Z. Zhou, M. Gong, and X. Tang, "Special Report on Deformation Failure Mechanism and Reinforcement Measures of Surrounding Rock of Underground Jinping-I Hydropower Cave Group in Yalong Hydropower Station, Sichuan Province," (Chengdu Survey, Design and Research Institute of China Hydropower Engineering Consulting Group, 2009): 1–100.

25. Z. Li, Z. Zhou, X. Tang, C. Liao, and Q. Chen, "Stability Analysis and Considerations of Underground Powerhouse Caves Group of Jinping I Hydropower Station," *Chinese Journal of Rock Mechanics and Engineering* 28 (2009): 2167–2175.

26. S. Huang, J. Wang, and X. Ding, "Stability and Control for Underground Caves of Jinping I Hydropower Station Based on Unloading Evolution of Layered Rock Mass," *Chinese Journal of Rock Mechanics and Engineering* 30 (2011): 2203–2216.

27. G. He, C. S. Jiang, Y. C. Lei, W. Liao, and B. Li, "Study on Unloading Relaxation Characteristics for Rock Masses Under High Geostress," *Applied Mechanics and Materials* 638–640 (2014): 594–600.

28. W. Liao, G. He, H. Xu, and X. Deng, "Detection on Time-Effect of Rock Relaxation Under High-Stressed Ground Condition," *Chinese Journal of Engineering Geophysics* 8 (2011): 609–615.

29. J. Yang, C. Chen, and Z. Liu, "Deformation and Failure Laws of Underground Cave Rock Mass in High Ground Stress," *Yangtze River People* 47 (2016): 37–41.

30. J. Yang, Z. Liu, and S. Huang, "Relaxation Depth and Supporting Time of Underground Powerhouse Surrounding Rock Under High Geostress at Jinping I Hydropower Station," *Journal of Engineering Geology* 24 (2016): 775–787.

31. W. Tong, "*Study on Working Behavior of Underground Cavern Group in Large-Scale Hydropower Project*," [Google Scholar] Master's Thesis, (Hohai University, Nanjing, China, 2006).

32. Y. X. Tan, "*Stability Analysis of Surrounding Rock of Large Underground Cavern Based on ABAQUS*," [Google Scholar] Master's Thesis, (Donghua University of Technology, Nanchang, China, 2016).

33. S. J. Deng, X. M. Lu, and X. Y. Huang, "A Brief Introduction to the Stability Analysis Method of Surrounding Rock of Underground Cavern," *Geological Exploration* 49 (2013): 541–547, [Google Scholar].

34. S. C. Bandis, G. Vardakis, N. Barton, and M. A. Addis, "Instability and Stress Transformations Around Underground Excavations in Highly Stressed Anisotropic Media," in *Proceedings of the Isrm International Symposium*, (Pau, France: OnePetro, [Google Scholar], 1989).

35. J. Zeng, Q. Sheng, and J. C. Tang, "Comparative Analysis of Layout Scheme of Underground Powerhouse Under Complex Geological Structure," *Journal of Underground Space and Engineering* 1 (2007): 105–109+113, [Google Scholar].

36. Q. Yang, X. Chen, and W. Y. Zhou, "Elastoplastic Damage Model and Deformation Localization Analysis of Rock and Soil Materials," *Chinese Journal of Rock Mechanics and Engineering* 21 (2004): 3577–3583, [Google Scholar].

37. X. Chen, Q. Yang, and W. Y. Zhou, "Plastic Damage Model of Rock and Soil Materials and Deformation Localization Analysis of Arch Dam," *Rock and Soil Mechanics* 5 (2007): 865–870, [Google Scholar].

38. J. H. Li and J. S. Yang, "Elastoplastic Nonlinear Finite Element Analysis of Rock Damage," *Chinese Journal of Rock Mechanics and Engineering* 6 (2000): 707–711, [Google Scholar].

39. G. Meng, Y. Fan, and Y. Jiang, "Key Rock Mechanical Problems and Measures for Huge Caves of Baihetan Hydropower Plant," *Chinese Journal of Rock Mechanics and Engineering* 35 (2016): 2549–2560.

40. A. Sharafat, W. A. Tanoli, M. U. Zubair, and K. M. Mazher, "Digital Twin-Driven Stability Optimization Framework for Large Underground Caverns," *Applied Sciences* 15, no. 8 (2025): 4481.

41. W. A. Tanoli, A. Ullah, A. Sharafat, and E. M. H. Ismaeil, "A Multi-Model BIM-Based Framework for Integrated Digital Transformation of Design to Construction of Large Complex Underground Caverns," *Buildings* 15, no. 16 (2025): 2834.

42. Q. Muhammad Waleed, R. W. Azfar Khan, A. Sharafat, W. Arshad Tanoli, M. U. Zubair, and H. J. Qureshi, "Development of BIM-Based Tunnel Information Modeling Prototype for Tunnel Design," *Advances in Civil Engineering* 2024, no. 1 (2024): 8118578.

43. A. Sharafat, K. Latif, S. Park, and J. Seo, "Digital Twin-Driven Optimization of Blast Design for Underground Construction," in *Proceedings of the KSCE Convention Conference and Civil Expo, Busan, Republic of Korea* (2022): 1-2

44. A. Sharafat, K. Latif, M. S. Khan, and J. Seo, "Development of BIM-IFC Standard Data Model Framework for Rock Support of Drill-and-Blast Tunnelling Projects," in *Proceedings of the KSCE Convention Conference and Civil Expo, Jeju, Republic of Korea* (2020): 536-537

45. Y. Jiao, X. Zhang, and T. Li, *DDARF Method for Simulating the Whole Failure Process of Jointed Rock Mass* (Science Press, 2010): 2–15.

46. Y.-Y. Jiao, X.-L. Zhang, H.-Q. Zhang, and G.-H. Huang, “A Discontinuous Numerical Model to Simulate Rock Failure Process,” *Geomechanics and Geoengineering* 9, no. 2 (2014): 133–141, [Google Scholar] [CrossRef].

47. Z. S. Wang, “*Study on Mechanism and Discontinuous Deformation Analysis of Hydraulic Fracturing of Rock*,” *Ph.D. Thesis*, ([Google Scholar], Shandong University, Jinan, China, 2019).

48. L. M. Wang, “*Finite Element Meshing Automation System for Specific Component*,” *Ph.D. Thesis*, ([Google Scholar], Shandong University, Jinan, China, 2017).

49. H.-P. Ma and N. N. N. Daud, “Jointed Rock Failure Mechanism: A Method of Heterogeneous Grid Generation for DDARF,” *Applied Sciences* 12, no. 12 (2022): 6095.

50. J. Chen, L. Li, X. Wan, D. Fang, and Y. Buyue, “Stress-Induced Brittle Failure of Surrounding Rock Mass and Its Engineering Countermeasures in the Baihetan Underground Powerhouse,” *IOP Conference Series: Earth and Environmental Science* 570 (2020): 052020.

51. National Energy Administration, *Technical Code for Underground Project Geological Investigation of Hydropower and Water Resources: DL/T5415-2009* (China Electric Power Press, 2009): 1–150.

52. W. Wang, G. Liu, Q. Su, and R. Han, “Analysis of Excavation Procedure and Stability in Jointed Rock Masses of Large Underground Caves,” in *Proceedings of the Application of Intelligent Systems in Multi-Modal Information Analytics Conference, MMIA, Advances in Intelligent Systems and Computing*, (Cham, Switzerland, 2019).

53. H.-P. Ma, N. N. N. Daud, Z. M. Yusof, W. Z. Yaacob, and H.-J. He, “Stability Analysis of Surrounding Rock of an Underground Cave Group and Excavation Scheme Optimization: On an Optimized DDARF Method,” *Applied Sciences* 13, no. 4 (2023): 2152.

54. Y. Wang and S. Liu, “Construction Prediction Analysis and Information Management of Excavation of Large Underground Cavern Groups,” *Engineering Journal Series* 3 (2007): 35–40.